Journal of the European Ceramic Society 41 (2021) 5170–5175

Contents lists available at ScienceDirect

Journal of the European Ceramic Society

journal homepage: www.elsevier.com/locate/jeurceramsoc

Novel low-ε_r MGa_2O_4 (M = Ca, Sr) microwave dielectric ceramics for 5 G antenna applications at the Sub-6 GHz band

Bing Liu [a,b,*], Ke Sha [a], Meng Fei Zhou [a], Kai Xin Song [a], Yu Hui Huang [b], Cheng Chao Hu [c]

[a] College of Electronic Information and Engineering, Hangzhou Dianzi University, Hangzhou, China
[b] School of Materials Science and Engineering, Zhejiang University, Hangzhou, China
[c] College of Materials Science and Engineering, Liaocheng University, Liaocheng, China

ARTICLE INFO

Keywords:
Gallates
Microwave dielectric properties
Sub-6GHz
Antenna

ABSTRACT

Two novel low-ε_r gallates MGa_2O_4 (M = Ca, Sr) have been synthesized via a standard solid-state reaction method. According to the X-ray diffraction results, $CaGa_2O_4$ crystallizes in space group $Pna2_1$ with an orthorhombic symmetry, while $SrGa_2O_4$ belongs to the monoclinic $P2_1/c$ system. Both ceramics show ever-improving microstructures with the increasing sintering temperature. The optimal microwave dielectric properties (ε_r = 9.2, Qf = 66,000 GHz, τ_f =–85 ppm/°C for $SrGa_2O_4$ and ε_r = 10.6, Qf = 15,400 GHz, τ_f =–58 ppm/°C for $CaGa_2O_4$) are obtained when sintered at 1275 °C. A patch antenna is fabricated using $SrGa_2O_4$ ceramics as the substrate, which realizes a return loss of –19.94 dB and total efficiency of –1.38 dB (72.8 % in power ratio) at 4.84 GHz. The exceptional performances indicate that $SrGa_2O_4$ ceramics are promising candidates for antenna applications at the Sub-6 GHz band.

1. Introduction

With the dramatic growth of wireless communication demands, the amount of data utilization increases remarkably, and the spectrum deficiency has become a challenging issue. The fifth-generation cellular wireless system (5 G), succeeding the 4 G LTE networks that we've been connecting to since 2010, offers prominent features such as high speed, high capacity, low latency, etc. [1–3]. Among the frequency bands used in 5 G technologies, the low-frequency band (<1 GHz) has been widely used in the 2/3/4 G systems. The high-frequency band in the millimeter-wave range (MmWave band) is still nascent as it covers very short ranges and is currently expensive to implement. The middle-frequency band (~3–6 GHz) or the so-called Sub-6 GHz band appeals to be an ideal middle ground between existing network backbones and boosts capacity like the MmWave band [4]. In 2015, Huawei proposed bands below 6 GHz as the primary working frequencies of 5 G and demonstrated a 5 G testbed working on the Sub-6 GHz band. In 2017, the Ministry of Industry and Information Technology of China officially assigned 3.4–3.6 GHz and 4.8–5.0 GHz as the working frequencies of commercial 5 G applications. At present, the Sub-6 GHz technology has occupied the largest market share of 5 G communications.

Low latency is one of the key aspects of the 5 G technologies and will likely be proved as one of the most significant upgrades over the older techs. Latency depends largely on the delay time (t_d) caused by the signal propagation in the dielectric materials. To shorten the signal delay time, materials with a low dielectric constant (ε_r < 15) have become the research focus since t_d is proportional to $\sqrt{\varepsilon_r}$ [5–7]. On the other hand, at higher frequencies, the dielectric loss increases significantly due to the increased wavenumbers. Hence, a high quality factor ($Q = 1/tan\delta$) is another requirement for the applications in the 5 G systems [5,8].

Aluminates are typical low-ε_r materials owing to the low ionic polarizability of Al^{3+} (0.79 $Å^3$) [9]. Among aluminates, AAl_2O_4 (A = Zn, Mg) spinel ceramics exhibit excellent microwave dielectric properties (ε_r = ~ 8.5, Qf = 56,000 ~ 105,000 GHz, τ_f = ~ –70 ppm/°C) and are referred to as one of the most promising low-ε_r materials [10,11]. To further explore the physical nature of AAl_2O_4 compounds, Yi et al. reported excellent performances (ε_r = 8.9, Qf = 91,350 GHz, τ_f =–55 ppm/°C) in $CaAl_2O_4$ ceramics as well [12,13]. The similar performances between $CaAl_2O_4$ and the spinels should be attributed to the similar radius between Ca^{2+} (1.0 Å) and Zn^{2+} (0.74 Å)/Mg^{2+} (0.72 Å). Meanwhile, further increasing of the radius of A^{2+} to 1.18 Å leads to structural change and symmetry breaking for $SrAl_2O_4$ ceramics, and the microwave dielectric properties are barely acceptable [14].

* Corresponding author at: College of Electronic Information and Engineering, Hangzhou Dianzi University, Hangzhou, China.
E-mail address: liubing@hdu.edu.cn (B. Liu).

https://doi.org/10.1016/j.jeurceramsoc.2021.04.033
Received 25 January 2021; Received in revised form 13 April 2021; Accepted 15 April 2021
Available online 19 April 2021

On the other hand, Ga and Al elements belong to the same group, which have similar physical/chemical properties. Moreover, gallates like $ZnGa_2O_4$ (*Qf* ~ 94,600 GHz) [15], $MgGa_2O_4$ (*Qf* ~ 117,000 GHz) [16], $LaGaO_3$ (*Qf* ~ 97,000 GHz) [17] generally exhibit higher *Qf* values as compare to their aluminate counterparts like $ZnAl_2O_4$ (*Qf* ~ 56,000 GHz) [10], $MgAl_2O_4$ (*Qf* ~ 105,000 GHz) [11], $LaAlO_3$ (*Qf* ~ 68,000 GHz) [18]. Meanwhile, the structural evolution and microwave dielectric properties in MGa_2O_4 (M = Ca, Sr) ceramics are still unclear, which is fundamental for their potential applications in the 5 G systems.

In this study, the sintering behavior, crystal structure, and microstructure of MGa_2O_4 ceramics are systematically investigated, together with their effects on the microwave dielectric properties. Meanwhile, a microstrip patch antenna using $SrGa_2O_4$ ceramics as the substrate is fabricated to reveal their applications at the Sub-6 GHz frequency range.

2. Experimental procedure

$CaGa_2O_4$ (CGO) and $Sr_2Ga_2O_4$ (SGO) ceramics were prepared via the solid-state reactions of high-purity starting powders of $CaCO_3$ (99.99 %, Aladdin Chemical Reagent Co., Ltd, China), $SrCO_3$ (99.95 %, Aladdin Chemical Reagent Co., Ltd, China), and Ga_2O_3 (99.99 %, Aladdin Chemical Reagent Co., Ltd, China). The stoichiometric powders were ball-milled in the ethanol media for 6 h. After drying, the mixtures were heated at 1100 °C for 3 h and then ground and further pressed into cylindrical pellets of 12 mm in diameter and 5 mm in height. Finally, the green pellets were sintered in the temperature range of 1200–1300 °C for 3 h to obtain the dense ceramics. For antenna substrate applications, the calcined powder was placed into a square die with a dimension of 20 × 20 cm and pressed under a uniaxial pressure of 200 MPa. The dry pressed green disk was then sintered at 1250 °C for 3 h to achieve similar densification with the pellets. Owing to the shrinkage during sintering, the dimensions of the sintered SGO ceramics were 17.3 × 17.3 × 1.13 mm.

X-ray diffraction patterns (XRD) of MGa_2O_4 ceramics were collected using a Bruker D8 diffractometer. XRD data for Rietveld refinement was recorded in the range of 10−120° with a step size of 0.02° and a counting time of 1.5 s. Rietveld refinements were carried out using a Fullprof software. The refined parameters sequence was the scale factor, background, zero shift, lattice parameters, peak shape parameters, half-width parameters, atomic coordinates, and isotropic thermal factors. Room temperature Raman spectra were collected using an HR-800 LabRaman device. The microstructures of the polished and thermally etched surface were observed using a Hitachi S-3400 scanning electron microscopy (SEM). The thermal etching process was carried out at a temperature 50 °C lower than the sintering temperature for 0.5 h. The design and simulation of the antenna were carried out using a Computer Simulation Technology (CST) software. The commercially available copper foil with a very thin layer of sticky glue on one side and a total thickness of 0.06 mm was used as the electrodes and pasted directly on the substrate. The antenna was fed by a 50Ω SMA (Subminiature version A) connector. The microwave dielectric properties and the antenna performances were evaluated using a Keysight N5234B network analyzer. The ε_r and τ_f were measured using the Hakki-Coleman method [19], and the *Qf* value was measured using the resonant cavity method [20].

3. Results and discussion

The XRD patterns of the sintered MGa_2O_4 ceramics are shown in Fig. 1. Both patterns can be well indexed and labeled based on the standard diffraction profiles of $CaGa_2O_4$ (JCPDS #00-16-0593) and $SrGa_2O_4$ (JCPDS #01-73-6002). No trace of additional diffraction peak is observed in SGO composition. While, a tiny peak corresponding to the existence of $CaGa_4O_7$ secondary phase is noticed in the Ca counterpart. The two patterns demonstrate disparate diffraction features despite their similar chemical compositions, indicating the diverse crystal structures

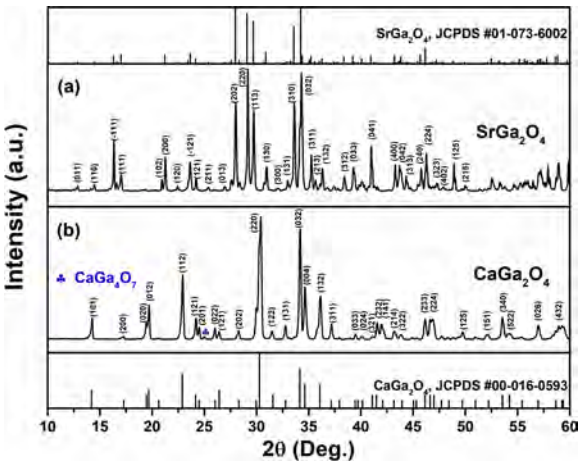

Fig. 1. The XRD patterns of (a) SGO and (b) CGO ceramics sintered at 1250 °C.

between SGO and CGO ceramics. Rietveld refinements of the XRD data are carried out to further determine the crystal structures. The crystal structures of the monoclinic $SrGa_2O_4$ with a space group of $P2_1/c$ and the orthorhombic $CaGa_2O_4$ with a space group of $Pna2_1$ are adopted as the initial structural models [21]. The calculated diffraction profiles and lattice parameters are given in Fig. 2 and Table 1, respectively. The calculated fraction of the $CaGa_4O_7$ secondary phase is 1.17 %. The refined XRD profiles are in good accordance with the measured ones, which can be verified from the low amplitudes of the blue difference lines. Besides, the satisfactory results of the calculated reliability factors (R_p = 5.03 %, R_{wp} = 7.87 % and χ^2 = 5.70 for CGO, and R_p = 8.40 %, R_{wp} = 6.32 % and χ^2 = 4.85 for SGO) further confirm the good consistency between the measured and calculated patterns.

The crystal structures of MGa_2O_4 ceramics derived from the refined results are shown in Fig. 3. According to the refined atomic positions listed in Table S1, there are two sets of A-site for alkali earth metal atoms

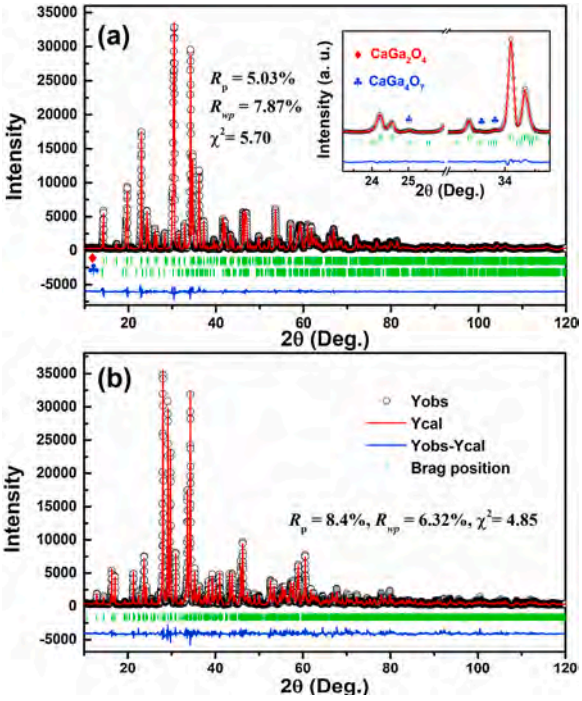

Fig. 2. The measured (black circles) and Rietveld refined (red lines) XRD patterns of (a) CGO and (b) SGO ceramics. (For interpretation of the references to colour in this figure legend, the reader is referred to the web version of this article).

Table 1
The refined lattice parameters of MGa_2O_4 ceramics.

Compositions	Space group	Lattice parameters				
		a (Å)	*b* (Å)	*c* (Å)	*β*	α=γ
$SrGa_2O_4$	$P2_1/c$	8.3767 (5)	8.9969 (6)	10.6826 (7)	93.9307°	90°
$CaGa_2O_4$	$Pna2_1$	10.3480 (2)	7.7463 (2)	9.1205 (2)	90°	90°

(Sr/Ca) and four possible B-sites for Ga atoms. The Ca and Sr atoms are coordinated by seven and six oxygen atoms, respectively, forming edge-sharing [CaO_7] and [SrO_6] polyhedrons. The crystal structure of SGO is constructed from a fully polymerized network of [GaO_4] tetrahedrons. All the Ga atoms are bonded with four adjacent O atoms. For CGO composition, the $Ga_{(4)}$ atom is in fivefold coordination, and a prolonged Ga-O bond with a value of 2.9809 Å is noticed. The rest of the Ga atoms are located inside the [GaO_4] tetrahedrons, with typical Ga-O bond lengths of approximately 1.88 Å.

The Raman spectra of MGa_2O_4 ceramics are recorded and shown in Fig. 4. The Raman spectra of the two compositions are different, which corresponds to their diverse crystal structures. Based on the group-theoretical analysis, the Raman active modes of CGO and SGO ceramics can be written as follows [22]:

$$\Gamma(\mathrm{CGO}) = \Gamma(\mathrm{SGO}) = 42A_g + 42B_g$$

The number of the recorded Raman active modes is much less than the predicted one, which should be related to the following reasons: (i) some modes are too weak to be detected, (ii) the cross-coverage of Raman peaks may obscure some others [23,24]. According to the previous studies on gallates, the Raman spectra of MGa_2O_4 ceramics can be divided into three regions, namely the low (below 400 cm^{-1}), medium (400−600 cm^{-1}), and high-frequency region (above 600 cm^{-1}) [25,26]. The low-frequency modes are caused by the rotational modes of the [GaO_4] tetrahedrons and the translational movements of the [GaO_4] unit and M atoms. The bending vibrations of the O-Ga-O bond mainly determine the medium-frequency part. The high-frequency Raman peaks are derived from the overlapping effects between the bending vibration and the symmetric stretching of the O-Ga-O bond [27]. For $CaGa_2O_4$ ceramics, the low-frequency modes at 190 cm^{-1}, 235 cm^{-1}, and 283 cm^{-1} are attributed to the displacements of the apical oxygen and Ca atoms [28]. The medium-frequency modes at 486 cm^{-1} and 541 cm^{-1} correspond to the bending modes of the O-Ga-O bridges [29]. The mode at 590 cm^{-1} is related to the superposition of the O-Ga-O vibration [30]. The high-frequency mode at 625 cm^{-1} is originated from the stretching vibration in the [GaO_4] tetrahedron [29].

Fig. 5 shows the SEM images and grain size distributions of MGa_2O_4 ceramics. At the sintering temperature of 1200 °C, the CGO and SGO ceramics present porous microstructures with relatively small average grain sizes of 1.5 μm and 4.5 μm, respectively (see Fig. S1 in the supporting information). With increasing sintering temperature, dense microstructures with closely packed grains and similar grain morphologies are observed in both compositions. A gradual increase in grain size is observed with increasing sintering temperature, which should be attributed to the increasing driving force of grain growth. Meanwhile, the grain sizes of SGO ceramics are overall larger than those of CGO.

The relative density of MGa_2O_4 ceramics as a function of the sintering temperatures is plotted in Fig. 6(a). At 1200 °C, the densities of both ceramics are relatively low, which correspond to the porous microstructures. Both curves indicate upward changing trends with the increasing sintering temperature until they reach the maximum values at 1300 °C. Moreover, the relative densities of higher than 95 % are obtained when sintered at above 1250 °C, which are in good agreement with the dense microstructures shown in the SEM images. The microwave dielectric properties of the present ceramics are shown in Fig. 6 (b–d). The ε_r of SGO ceramics increases monotonously from 8.87 at 1200 °C to 9.26 at 1300 °C, consistent with the variation trend of the relative density. Similarly, for the Ca counterpart, the ε_r increases from 9.83 to 10.6 and decreases slightly to 10.5 at 1300 °C. The dielectric constant can be corrected (denote as ε_{cor}) to exclude the effects of porosity (*P*) using the following Bosman-Having equation [31,32].

$$\varepsilon_{cor} = \varepsilon_r(1 + 1.5P) \quad (1)$$

The calculated ε_{cor} values are ~9.7 for SGO and ~11 for CGO. Besides, the porosity corrected values remain stable with increasing sintering temperature, indicating that the porosity plays the dominating

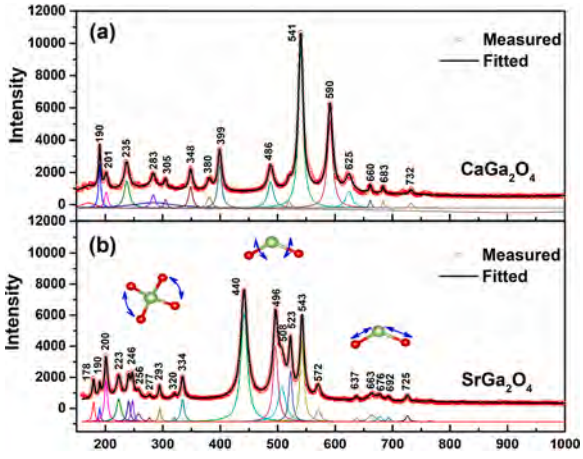

Fig. 4. The room temperature Raman spectra of (a) CGO and (b) SGO ceramics.

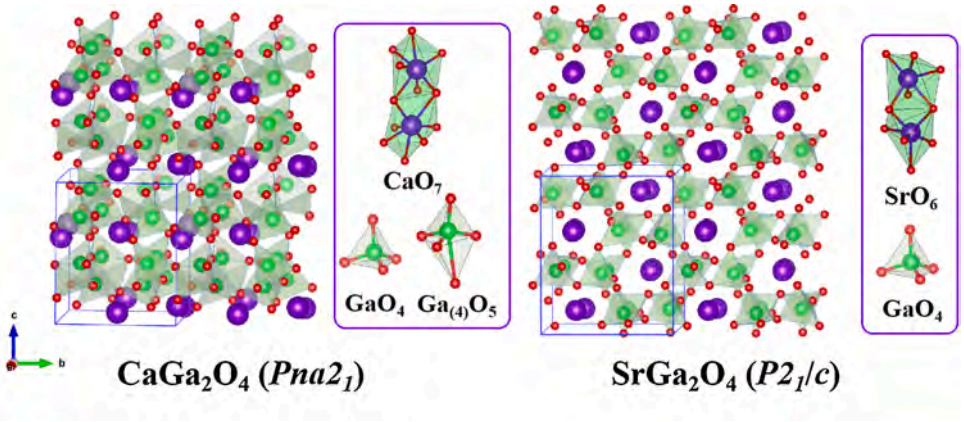

Fig. 3. The crystal structures of MGa_2O_4 ceramics.

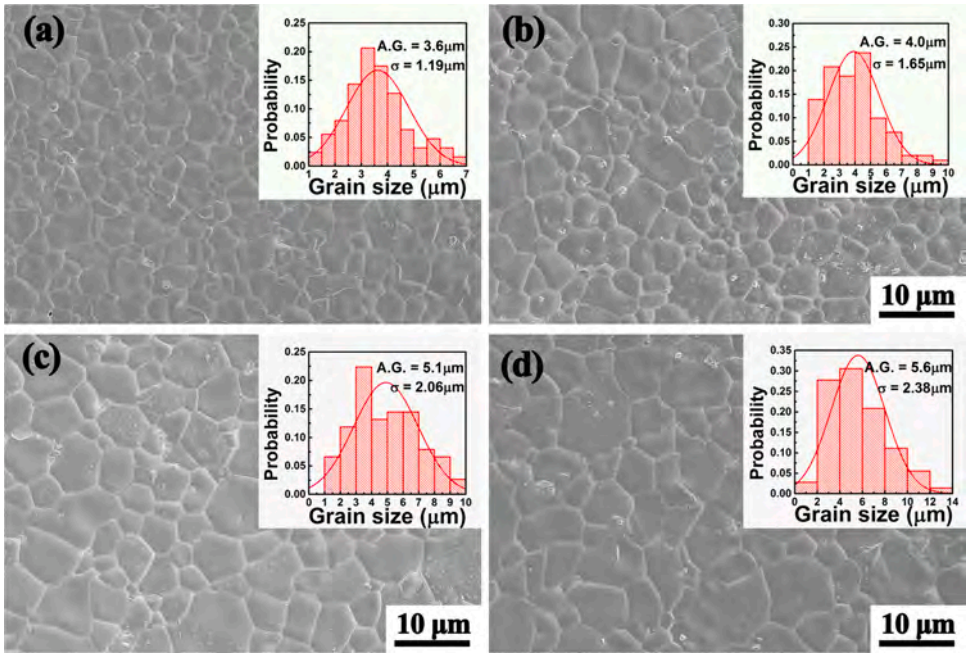

Fig. 5. SEM images and grain size distributions of MGa_2O_4 ceramics sintered at various temperatures. (a) CGO@1250 °C, (b) CGO@1300 °C, (c) SGO@1250 °C, and (d) SGO@1300 °C.

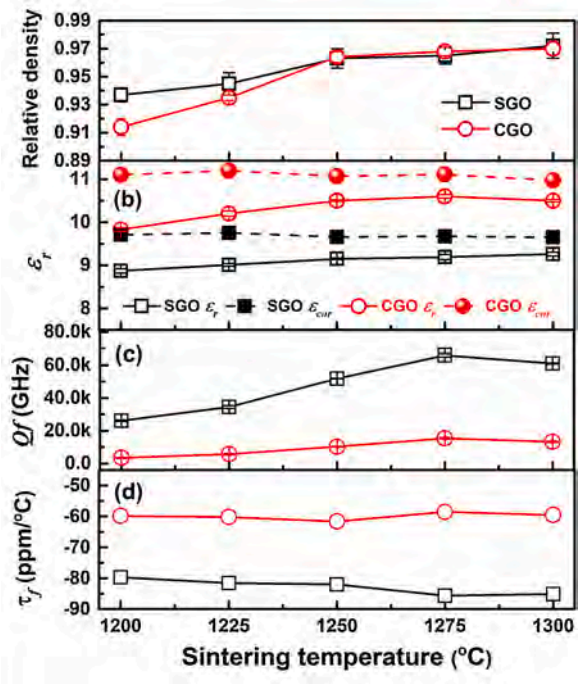

Fig. 6. The variations of the (a) relative density, (b) ε_r, (c) Qf, and (d) τ_f values of MGa_2O_4 ceramics with the sintering temperature.

role in determining the ε_r.

The Qf values of MGa_2O_4 ceramics sintered at various temperatures are shown in Fig. 6(c). The Qf values increase with the sintering temperature until the maximum values (66,000 GHz for SGO and 15,400 GHz for CGO) are attained at 1275 °C. The Qf values of SGO ceramics are much larger than those of the Ca counterpart. This should be attributed to the existence of the $CaGa_4O_7$ secondary phase in $CaGa_2O_4$ ceramics, as the impurities are notoriously harmful to the quality factor [33][34].

The τ_f values indicate less sensitive variation trends with the sintering temperature. The τ_f values of SGO and CGO ceramics fluctuate at approximately –82 ppm/°C and –60 ppm/°C, respectively. The bond valence has been widely accepted as a valuable tool in correlating the structural parameters with the τ_f values. The bond valences (V_{ij}) of the M-site and Ga-site of the present ceramics are calculated using the following equations [23,35].

$$V_{ij} = \sum_j v_{ij} \tag{2}$$

$$v_{ij} = \exp\left[\frac{R_{ij} - d_{ij}}{b}\right] \tag{3}$$

where, R_{ij} denotes the bond valence parameter between atoms i and j, d_{ij} is the bond length (listed in the supporting information), and b is a constant value of 0.37 Å [35]. The calculated bond valences of the present ceramics are listed in Table 2. According to the bond valence theory [36], the lower the bond valence, the lower energy needs to recover the deformation of oxygen polyhedron, ultimately leads to the increase of $|\tau_f|$. Hence, the lower τ_f value of SGO ceramics should be ascribed to its lower bond valence (14.77) than that of CGO (15.055). The microwave dielectric properties of the present ceramics are summarized in Table S3. The optimal microwave dielectric properties are obtained as follows ($\varepsilon_r = 9.2$, $Qf = 66{,}000$ GHz, $\tau_f = -85$ ppm/°C for SGO, and $\varepsilon_r = 10.6$, $Qf = 15{,}400$ GHz, $\tau_f = -58$ ppm/°C for CGO). The ε_r of the present ceramics are similar to those of the spinel $MgGa_2O_4$/$ZnGa_2O_4$ ceramics, while the Qf values are inferior [15,16]. To further tune the negative τ_f values towards zero, an easy and effective strategy is to combine other composites with opposite τ_f values [37,38]. In this study, $CaTiO_3$ with a large positive τ_f value of approximately 800 ppm/°C is added into $SrGa_2O_4$ forming (1-x)$SrGa_2O_4$–$x CaTiO_3$ ($x = 0.05$, 0.10, and 0.15) composite ceramics. The XRD patterns and microwave dielectric properties of the composite ceramics are shown in Fig. S2. The XRD results indicate that no chemical reaction occurs between the two composites. As expected, a near-zero τ_f value of –3.1 ppm/°C is obtained in the $0.9SrGa_2O_4$-$0.1CaTiO_3$ ceramics, with $\varepsilon_r = 11.7$ and $Qf = 33{,}700$ GHz.

A microstrip patch antenna is fabricated using SGO ceramics as the dielectric substrate to further identify their antenna applications. The

Table 2
The calculated bond valences of MGa_2O_4 ceramics.

	$R_{Ca\text{-}O}$ (Å)	$R_{Sr\text{-}O}$ (Å)	$R_{Ga\text{-}O}$ (Å)	b (Å)	$\sum V_{Ca\text{-}O}$	$\sum V_{Sr\text{-}O}$	$\sum V_{Ga\text{-}O}$	$\sum$
$CaGa_2O_4$	1.967		1.730	0.37	3.859	\	11.196	15.055
$SrGa_2O_4$	\	2.118	1.730	0.37	\	4.571	10.199	14.77

designed dimensions and the photographic image validating the proposed design are shown in Fig. 7(a). The measured and simulated S11 curves of the proposed antenna are demonstrated in Fig. 7(b). The measured S11 curve presents a good return loss of –19.94 dB at the resonant frequency of 4.84 GHz, which conforms to the antenna requirements operating at the targeted Sub-6 GHz band. Overall, the measured and simulated S11 curves are in good agreement, where the simulated resonant frequency and return loss of the proposed antenna are 4.80 GHz and–23.74 dB, respectively. The difference could be ascribed to the manufacturing process's accuracy, impendence mismatch, and SMA connector's soldering [39–42]. The VSWR (Voltage Standing Wave Ratio) of commercial antenna products is typically in the range of 1∼1.5 dB. The lower the VSWR, the better the antenna performance. The figure inset plots the measured VSWR curve of the fabricated antenna, and the VSWR value at 4.84 GHz is 1.22 dB, which is suitable for 5 G antenna applications.

The simulated 3D far-field gain pattern is shown in Fig. 7(c). The electromagnetic signal mainly propagates along the Z direction with a maximum gain of 2.9dBi. The maximum gain is also verified from the radiation patterns of the two principal planes (E and H planes) shown in Fig. 7(d). The simulated total efficiency of the SGO patch antenna is plotted in Fig. 7(e), where the maximum value of –1.38 dB is obtained. An antenna's efficiency denotes the power radiated from the antenna (P_2) relative to the power delivered to the antenna (P_1). Decibel (dB) is related to the power ratio (P_2/P_1) using the following equation [39].

$$\mathrm{dB} = 10 \times \lg(P_2/P_1) \tag{4}$$

Based on the equation, the converted efficiency of the antenna is 72.8 %. The efficiency is affected by various parameters, such as the impedance mismatch loss, the conduction loss due to electrodes' finite conductivity, and the dielectric loss of the substrate. For commercial antennas applied in mobile phones and WiFi products, the required efficiency is typically in the range of 20 %–70 % (–7 ∼ –1.5 dB) [34,43]. Hence, based on the above discussion, SGO ceramics exhibit exceptional microwave dielectric properties and can be applied as promising substrates for 5 G antenna applications.

4. Conclusions

MGa_2O_4 (M = Ca, Sr) ceramics have been prepared via a standard solid-state sintering method. The XRD and Rietveld refinement results indicate that $SrGa_2O_4$ crystallizes in the $P2_1/c$ symmetry, while $CaGa_2O_4$ crystal belongs to the space group $Pna2_1$. The SEM images indicate ever-improving microstructures with the increasing sintering temperature. The microstructure optimization mainly determines the improvement of the ε_r and Qf, and the τ_f is closely related to the bond valence. The optimal microwave dielectric properties of MGa_2O_4 ceramics are obtained as follows: ε_r = 9.2, Qf = 66,000 GHz, τ_f =–85 ppm/°C for $SrGa_2O_4$ and ε_r = 10.6, Qf = 15,400 GHz, τ_f =–58 ppm/°C for $CaGa_2O_4$. A square patch antenna is designed and fabricated using $SrGa_2O_4$

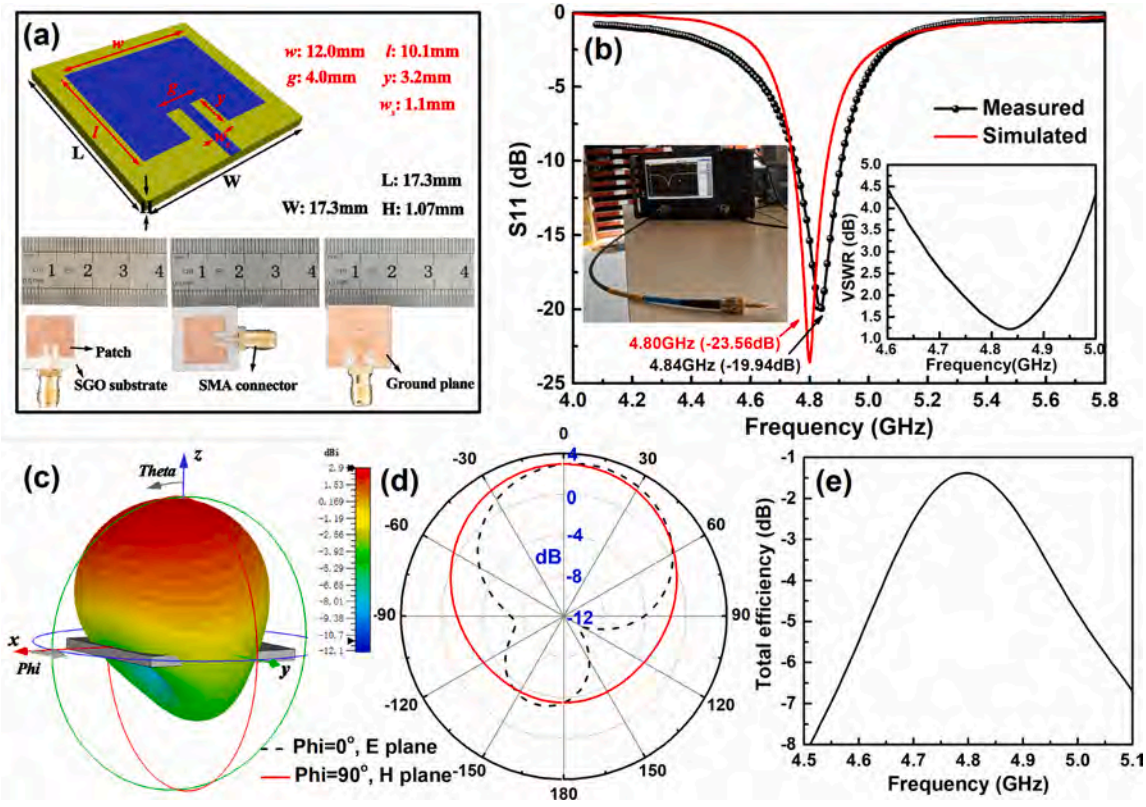

Fig. 7. (a) The geometries, front and rear views of the fabricated microstrip patch antenna. (b) The simulated and measured S11 curves of the proposed antenna, the inset figure shows the measured VSWR curve of the antenna. The simulated (c) 3D far-field gain pattern and (d) the radiation patterns in the E and H planes. (e) The simulated total efficiency as a function of the frequency.

ceramic as the dielectric substrate. The fabricated antenna presents good radiation coefficients at the targeted Sub-6 GHz band, with a return loss of –19.94 dB and a VSWR of 1.22 dB at 4.84 GHz. The proposed antenna's total efficiency is simulated to be –1.38 dB (72.8 % in power ratio). Accordingly, $SrGa_2O_4$ ceramics are expected as promising candidates for 5 G antenna applications.

Declaration of Competing Interest

The authors declare no conflicts of interest.

Acknowledgment

The authors greatly appreciate the finical supports from the National Natural Science Foundation of China under grant number (51802062, 51802280) and the Postdoctoral Research Foundation of Zhejiang Province under grant number (ZJ2020008).

Appendix A. Supplementary data

Supplementary material related to this article can be found, in the online version, at doi:https://doi.org/10.1016/j.jeurceramsoc.2021.04.033.

References

[1] J.G. Andrews, S. Buzzi, W. Choi, S.V. Hanly, A. Lozano, A.C.K. Soong, J.Z.C. Zhang, What will 5G be? IEEE J. Sel. Area Comm. 32 (2014) 1065–1082.
[2] M.D. Hill, D.B. Cruickshank, Ceramic materials for 5G wireless communication systems, Am. Ceram. Soc. Bull 98 (2019) 20–25.
[3] M. Anab, M.I. Khattak, S.M. Owais, A.A. Khattak, A. Sultan, Design and analysis of millimeter wave dielectric resonator antenna for 5G wireless communication systems, Prog. Electromagn. Res. 98 (2020) 239–255.
[4] Y. Wu, J. Wang, S. Lai, X. Zhu, W. Gu, Transparent and flexible broadband absorber for the sub-6G band of 5G mobile communication, Opt. Mater. Express 8 (2018) 3351–3358.
[5] B. Liu, L. Li, K.X. Song, M.M. Mao, Z. Lu, G. Wang, L. Li, D. Wang, D. Zhou, A. Feteira, I.M. Reaney, Enhancement of densification and microwave dielectric properties in LiF ceramics via a cold sintering and post-annealing process, J. Eur. Ceram. Soc. 41 (2021) 1726–1729.
[6] H. Ohsato, J. Varghese, A. Kan, J.S. Kim, I. Kagomiya, H. Ogawa, M.T. Sebastian, H. Jantunen, Volume crystallization and microwave dielectric properties of indialite/cordierite glass by TiO_2 addition, Ceram. Int. 47 (2021) 2735–2742.
[7] D. Zhou, L.X. Pang, D.W. Wang, Z.M. Qi, I.M. Reaney, High quality factor, ultralow sintering temperature $Li6B_4O_9$ microwave dielectric ceramics with ultralow density for antenna substrates, ACS Sustain. Chem. Eng. 6 (2018) 11138–11143.
[8] W.B. Hong, L. Li, H. Yan, S.Y. Wu, H.S. Yang, X.M. Chen, Room-temperature-densified H_3BO_3 microwave dielectric ceramics with ultra-low permittivity and ultra-high Qf value, J. Materiomics 6 (2020) 233–239.
[9] R.D. Shannon, Dielectric polarizabilities of ions in oxides and fluorides, J. Appl. Phys. 73 (1993) 348–366.
[10] K.P. Surendran, N. Santha, P. Mohanan, M.T. Sebastian, Temperature stable low permittivity ceramic dielectrics in (1-x)$ZnAl_2O_4$-xTiO_2 system for microwave substrate applications, Eur. Phys. J. B 41 (2004) 301–306.
[11] K.P. Surendran, P.V. Bijumon, P. Mohanan, M.T. Sebastian, (1-x)$MgAl_2O_4$-xTiO_2 dielectrics for microwave and millimeter wave applications, Appl. Phys. A 81 (2005) 823–826.
[12] L. Yi, M.M. Mao, L. Li, X.M. Chen, Structures and microwave dielectric characteristics of compounds in vicinity of $CaNdAlO_4$ in CaO-Nd_2O_3-Al_2O_3 ternary system, Adv. Appl. Ceram. 112 (2013) 46–52.
[13] B. Liu, C.C. Hu, Y.H. Huang, H.B. Bafrooei, K.X. Song, Crystal structure, infrared reflectivity spectra and microwave dielectric properties of $CaAl_2O_4$ ceramics with low permittivity, J. Alloys. Compd. 791 (2019) 1033–1037.
[14] J.M. Perez-Mato, R.L. Withers, A.K. Larsson, D. Orobengoa, Y. Liu, Distortion modes and related ferroic properties of the stuffed tridymite-type compounds $SrAl_2O_4$ and $BaAl_2O_4$, Phys. Rev. B 79 (2009), 064111.
[15] J. Xue, S. Wu, J. Li, Synthesis microstructure and microwave dielectric properties of spinel $ZnGa_2O_4$ ceramics, J. Am. Ceram. Soc. 96 (2013) 2481–2485.
[16] X. Wu, J. Xue, R. Wang, J. Li, Synthesis, characterization and microwave dielectric properties of spinel $MgGa_2O_4$ ceramic materials, J. Alloys. Compd. 585 (2014) 542–548.
[17] H. Zheng, GDC. Csete de Gyorgyfalva, I.M. Reaney, Microstructure and microwave properties of $CaTiO_3$-$LaGaO_3$ solid solutions, J. Mater. Sci. 40 (2005) 5207–5214.
[18] S.Y. Cho, I.T. Kim, K.S. Hong, Microwave dielectric properties and applications of rare earth aluminates, J. Mater. Res. 14 (1999) 114–119.
[19] D. Kajfez, A. Gundavajhala, Measurement of material properties with a tunable resonant cavity, Electron. Lett. 29 (1993) 1936–1937.
[20] B.W. Hakki, P.D. Coleman, A dielectric resonant method of measuring inductive capacitance in the millimeter range, IRE Trans. Microwave Theory Tech. 8 (1960) 402–410.
[21] S. Gražulis, D. Chateigner, R.T. Downs, A.F.T. Yokochi, M. Quirós, L. Lutterotti, E. Manakova, J. Butkus, P. Moeck, A. Le Bail, Crystallography Open Database–an open-access collection of crystal structures, J. Appl. Crystallogr. 42 (2009) 726–729.
[22] M.I. Aroyo, J.M. Perez-Mato, C. Capillas, E. Kroumova, S. Ivantchev, G. Madariaga, A. Kirov, H. Wondratschek, Bilbao crystallographic server: I. Databases and crystallographic computing programs, Z. Kristallogr. 221 (2006) 15–27.
[23] Y. Zhai, Y. Tang, J. Li, L. Duan, C. Su, A. Cao, C. Jin, L. Fang, Structure, Raman spectra and properties of two low-ε_r microwave dielectric ceramics $Ca_3B_2Ge_3O_{12}$ (B = Al, Ga), Ceram. Int. 46 (2020) 28710–28715.
[24] J. Zhang, R. Zuo, Phase structural transition and microwave dielectric properties in isovalently substituted $La_{1-x}Ln_xTiNbO_6$ (Ln = Ce, Sm) ceramics, Ceram. Int. 43 (2017) 7065–7072.
[25] V. Monteseguro, P. Rodríguez-Hernández, R. Vilaplana, F.J. Manjón, V. Venkatramu, D. Errandonea, V. Lavín, A. Munoz, Lattice dynamics study of nanocrystalline yttrium gallium garnet at high pressure, J. Phys. Chem. C 118 (2014) 13177–13185.
[26] K. Papagelis, J. Arvanitidis, E. Vinga, D. Christofilos, G.A. Kourouklis, H. Kimura, S. Ves, Vibrational properties of $(Gd_{1-x}Y_x)_3Ga_5O_{12}$ solid solutions, J. Appl. Phys. 107 (2010), 113504.
[27] S. Liu, S. Ma, S. Wang, Z. Ye, Exploring crystal-field splittings of Eu^{3+} ions in γ- and β-$SrGa_2O_4$, J. Lumin. 210 (2019) 155–163.
[28] R. Sopracase, G. Gruener, E. Olive, J.-C. Soret, Infrared study of the phonon modes in $PrMnO_3$ and $CaMnO_3$, Physica B 405 (2010) 45–52.
[29] M. Fumiaki, S. Sakka, Structure of PbO-Bi_2O_3-Ga_2O_3 glasses, J. Non-Cryst. Solids 134 (1991) 77–85.
[30] A.A. Kharlamov, R.M. Almeida, J. Heo, Vibrational spectra and structure of heavy metal oxide glasses, J. Non-Cryst. Solids 202 (1996) 233–240.
[31] A.J. Bosman, E.E. Havinga, Temperature dependence of dielectric constants of cubic ionic compounds, Phy. Rev. 129 (1963) 1593–1600.
[32] L. Li, W.B. Hong, S. Yang, H. Yan, X.M. Chen, Effects of water content during cold sintering process of NaCl ceramics, J. Alloys. Compd. 787 (2019) 352–357.
[33] B. Liu, Y.H. Huang, K.X. Song, L. Li, X.M. Chen, Structural evolution and microwave dielectric properties in $Sr_2(Ti_{1-x}Sn_x)O_4$ ceramics, J. Eur. Ceram. Soc. 38 (2018) 3833–3839.
[34] B. Liu, K. Sha, Y.Q. Jia, Y.H. Huang, C.C. Hu, L. Li, D. Zhou, K.X. Song, High quality factor cold sintered LiF ceramics for microstrip patch antenna applications, J. Eur. Ceram. Soc. 41 (2021) 4835–4840, https://doi.org/10.1016/j.jeurceramsoc.2021.03.052.
[35] N.E. Brese, M. O'keeffe, Bond-valence parameters for solids, Acta Crystallogr. 47 (1991) 192–197.
[36] A.M. Glazer, The classification of tilted octahedral in perovskites, Acta Crystallogr. 28 (1972) 3384–3392.
[37] C. Li, H. Xiang, M. Xu, Y. Tang, L. Fang, Li_2AGeO_4(A = Zn, Mg): Two novel low-permittivity microwave dielectric ceramics with olivine structure, J. Eur. Ceram. Soc. 38 (2018) 1524–1528.
[38] Y.H. Huang, B. Liu, K.X. Song, Microwave dielectric properties of temperature stable (1-x)$SrLaAlO_4$-xTiO_2 composite ceramics, Ceram. Int. 44 (2018) S125–S128.
[39] H. Xiang, J. Kilpijärvi, S. Myllymäki, H. Yang, L. Fang, H. Jantunen, Spinel-olivine microwave dielectric ceramics with low sintering temperature and high quality factor for 5 GHz WiFi antennas, Appl. Mater. Today 21 (2020), 100826.
[40] S.B. Roshni, S. Arun, M.T. Sebastian, P. Mohanan, K.P. Surendran, Low κ Mg_2SiO_4 ceramic tapes and their role as screen printed microstrip patch antenna substrates, Mater. Sci. Eng. B 264 (2021), 114947.
[41] P. Abhilash, S.B. Roshni, P. Mohanan, K.P. Surendran, A facile development of homemade substrate using 'quench free' glass-ceramic composite and printing microstrip patch antenna on it, Mater. Des. 137 (2018) 38–46.
[42] D.E. Bockelman, W.R. Eisenstadt, Combined differential and common-mode scattering parameters: theory and simulation, IEEE Trans. Micro. Theory 43 (1995) 1530–1539.
[43] D.C. Thompson, O. Tantot, H. Jallageas, G.E. Ponchak, M.M. Tentzeris, J. Papapolymerou, Characterization of liquid crystal polymer (LCP) material and transmission lines on LCP substrates from 30 to 110 GHz, IEEE Trans. Micro. Theory 52 (2004) 1343–1352.